GCN5L1 promotes diastolic dysfunction by inhibiting cardiac pyruvate oxidation

Dharendra Thapa[1,2,3 # $], Paramesha Bugga[1,2,3 #], Bellina A.S. Mushala[1,2,3], Janet R. Manning[1,2,3], Michael W. Stoner[1,2,3], Brenda McMahon[2], Xuemei Zeng[4], Pamela Cantrell[4], Nathan Yates[4], Bingxian Xie[3,5], Lia R. Edmunds[3,5], Michael J. Jurczak[3,5], and Iain Scott[1,2,3 *]

[1] Division of Cardiology, [2] Vascular Medicine Institute, [3] Center for Metabolism and Mitochondrial Medicine, [4] Biomedical Mass Spectrometry Center, and [5] Division of Endocrinology and Metabolism, Department of Medicine, University of Pittsburgh, Pittsburgh, PA.

[$] Present Address: Department of Exercise Physiology, West Virginia University School of Medicine, Morgantown, WV.

[#] These authors contributed equally to this work.

* Corresponding Author:
Iain Scott, PhD, FAHA, FCVS
Department of Medicine
University of Pittsburgh
BST E1259
200 Lothrop Street
Pittsburgh PA
15261
Email: iain.scott@pitt.edu
Tel: (412) 648-7691

Word Count (Main Text): 1309

Short title: PDH inhibition and cardiac diastolic dysfunction

Keywords: Pyruvate dehydrogenase, acetylation, diastolic dysfunction, heart failure, mitochondria

ABSTRACT

Left ventricular diastolic dysfunction is a structural and functional condition that may precede the development of heart failure with preserved ejection fraction (HFpEF). The etiology of diastolic dysfunction includes alterations in fuel substrate metabolism that negatively impact cardiac bioenergetics, and may precipitate the eventual transition to heart failure. To date, the molecular mechanisms that regulate early changes in fuel metabolism leading to diastolic dysfunction remain unclear. Here, we use a diet-induced obesity model and quantitative acetylproteomics to show that inhibitory lysine acetylation of the pyruvate dehydrogenase complex promotes energetic deficits and diastolic dysfunction in mouse hearts. Our findings suggest that changes in mitochondrial protein lysine acetylation represent a key component of diastolic dysfunction that precedes the development of heart failure.

INTRODUCTION

Left ventricular diastolic dysfunction is an independent pre-clinical predictor of all-cause mortality [1], and is a prerequisite for the diagnosis of heart failure with preserved ejection fraction (HFpEF) [2]. Diastolic dysfunction precedes the development of HFpEF, and tackling this condition at an early stage may represent a therapeutic opportunity to prevent progression to heart failure. While the etiology of the diastolic dysfunction is multifactorial, deleterious changes in cardiac energy metabolism underpin the development of both diastolic dysfunction and HFpEF [3,4]. Two studies on two recently developed murine models of HFpEF have reported maladaptive changes to the relative oxidation rates of fatty acids, ketones, and glucose in failing hearts [5,6], suggesting that this metabolic

phenotype is central to the development of cardiac dysfunction. Interestingly, the HFpEF phenotype in these two independent mouse models is also characterized by an increase in mitochondrial protein acetylation, a reversible posttranslational modification that is commonly linked to reduced metabolic enzyme activity [5,6]. Restoring normal mitochondrial protein acetylation through supplementation with either nicotinamide riboside (to stimulate SIRT3-mediated protein deacetylation) [5], or ketone bodies (which inhibit fatty acid uptake and utilization) [6], resulted in normalized cardiac bioenergetics and amelioration of the HFpEF phenotype [5,6].

These studies suggest that tight regulation of mitochondrial protein acetylation is required to prevent the development of HFpEF, and therefore approaches that reduce maladaptive protein hyperacetylation are potentially cardioprotective. Using a mouse model of constitutively reduced mitochondrial protein acetylation and quantitative acetylproteomics, we examined the metabolic mechanisms underlying protection from diastolic dysfunction in mice prior to the development of heart failure.

RESULTS

While the two HFpEF mouse studies referenced above used diet-based two-hit (high fat diet and the eNOS inhibitor L-NAME) [5] or three-hit (high fat diet, aging, and the mineralocorticoid ester desoxycorticosterone pivalate) [6] models to produce the HFpEF phenotype, long-term exposure to a high fat diet alone can promote diastolic dysfunction [7]. We therefore used a long-term high fat diet model to specifically examine diastolic dysfunction in a pre-HFpEF state. Wildtype (WT) and cardiomyocyte-specific GCN5L1 knockout (KO) mice (which display global reductions in mitochondrial

77 protein acetylation) [8] were placed on low fat (LFD; 10% fat) or high fat (HFD; 60% fat) diets for 30
78 weeks (**Figure 1A**), and heart structure and function were measured by ultrasonography (**Figure 1B**).
79 No changes in systolic function (left ventricle ejection fraction; LVEF) were observed on either diet
80 between WT and KO mice (**Figure 1C,D**). In contrast, WT mice displayed a significant increase in
81 E/e' ratio (a marker of diastolic dysfunction) [5] on a HFD, which was absent in acetylation-deficient
82 KO mice under the same conditions (**Figure 1E,F**).
83
84 To understand which mitochondrial metabolic pathways are regulated by GCN5L1-mediated
85 acetylation under conditions that promote diastolic dysfunction, we performed quantitative
86 acetylproteomics on HFD-fed WT and KO mice (**Figure 1G; Table S1**). Gene ontology analysis using
87 PANTHER demonstrated that enzymes involved in mitochondrial fatty acid oxidation and pyruvate
88 metabolism were among the top three pathways most affected by GCN5L1-regulated lysine
89 acetylation (**Figure 1H**).
90
91 To understand if one or both fuel metabolism pathways were disrupted in mice with diastolic
92 dysfunction, we performed Oroboros respirometry in cardiac tissue lysates from HFD-fed WT and KO
93 mice. Previous reports have shown that fatty acid oxidation is significantly modified in hyperacetylated
94 mitochondria from HFpEF-model mice [5,6]. However, we found here that ADP-stimulated state 3
95 respiration was not different between WT and KO samples given palmitate as a fuel substrate.
96 Instead, we observed a significant increase in ADP-stimulated state 3 respiration in KO tissues given
97 pyruvate as a fuel source, relative to their WT counterparts (**Figure 1I,J**). Combined, these data
98 indicate that a loss of pyruvate oxidation, rather than aberrant fatty acid oxidation, underpins the
99 energetic deficits that contribute to the development of diastolic dysfunction in this model.

The pyruvate dehydrogenase (PDH) complex regulates mitochondrial pyruvate utilization, and previous work has demonstrated that increasing PDH activity can reverse diastolic dysfunction in diabetic rodents [9,10]. Elevated PDH activity is commonly associated with a decrease in inhibitory phosphorylation at Ser-293 [5], however we detected no difference in PDH phosphorylation between WT and KO mice on either diet (**Figure 2A,C**). Instead, we found a significant increase in hyperacetylation of PDHA1 (a component of the PDH E1 enzyme) in HFD-fed WT mice relative to LFD controls, and a significant decrease in PDHA1 acetylation in both KO diet groups (**Figure 2B,D**). Consistent with this, PDH activity was significantly increased in KO mice on a long-term HFD, relative to both WT diet groups (**Figure 2E**), and PDHA1 acetylation status across all animal groups was negatively correlated with PDH activity by linear regression (R^2 = 0.3678; P = 0.037; **Figure 2F**). To verify these findings independently, we examined PDH activity and acetylation status in the human-derived AC16 cardiomyocyte cell model following shRNA-mediated GCN5L1 depletion. Knockdown of GCN5L1 in AC16 cells resulted in a ~40% increase in PDH activity, and a ~50% decrease in PDHA1 acetylation, without observed changes in total PDH abundance (**Figure 2G-L**). Combined, these data suggest that GCN5L1-mediated hyperacetylation of PDH, rather than inhibitory PDH phosphorylation, is a key driver of defects in pyruvate oxidation in the context of diet-induced diastolic dysfunction.

Finally, we sought to determine the specific effect of lysine hyperacetylation on PDH enzymatic activity. Published studies in the PhosphoSitePlus proteomics database (www.phosphosite.org) have identified five acetylation sites on human PDHA1 at K18, K39, K244, K321, and K336 (**Figure 2M**). We generated novel PDHA1 expression constructs, where each of these five lysines were replaced with either arginine (5KR; to mimic a non-acetylated state) or glutamine (5KQ; to mimic a

hyperacetylated state; **Figure 2N**), and expressed them in GCN5L1 knockdown AC16 cells (which represent a basal, non-acetylated state for endogenous PDHA1). PDH activity was significantly increased in non-acetylated PDHA1 5KR expressing cells relative to those overexpressing wildtype PDHA1 (**Figure 2O**). Conversely, PDH activity was significantly decreased in hyperacetylated PDHA1 5KQ expressing cells relative to those deficient in PDHA1 acetylation (**Figure 2O**). Together, these cell model data indicate that hyperacetylation of PDHA1 has a specific negative effect on PDH enzymatic activity in cardiac cells.

DISCUSSION

In conclusion, we show that inhibitory acetylation of PDHA1 drives reduced pyruvate utilization in a diet-based model of cardiac diastolic dysfunction. The inhibitory effect of PDH acetylation in diastolic dysfunction described here is consistent with its role in mouse models of heart failure with reduced ejection fraction (HFrEF), where miR-195-mediated downregulation of the deacetylase SIRT3 leads to increased acetylation of PDH subunits and decreased PDH enzymatic activity [12]. However, in this study we detected no differences in SIRT3 abundance in response to diet or genotype (data not shown), placing GCN5L1 at the center of mitochondrial acetylome regulation in this diastolic dysfunction model. Interestingly, the deletrious effect of global mitochondrial protein hyperacetylation in the development of HFpEF [5,6] sits at odds with its demonstrated lack of effect in mouse surgical models of HFrEF [13,14]. Further work will be required to determine whether the differences found reflect the etiology of the different models used, the site-specific nature of the acetylation sites modified on each protein, or whether the different mechanisms by which GCN5L1 and SIRT3 control mitochondrial protein acetylation status lead to different functional outcomes.

REFERENCES

[1] Redfield MM, Jacobsen SJ, Burnett JC Jr, Mahoney DW, Bailey KR, Rodeheffer RJ. Burden of systolic and diastolic ventricular dysfunction in the community: appreciating the scope of the heart failure epidemic. JAMA. 2003 Jan 8;289(2):194-202.

[2] Shah KS, Xu H, Matsouaka RA, Bhatt DL, Heidenreich PA, Hernandez AF, Devore AD, Yancy CW, Fonarow GC. Heart Failure With Preserved, Borderline, and Reduced Ejection Fraction: 5-Year Outcomes. J Am Coll Cardiol. 2017 Nov 14;70(20):2476-2486.

[3] Lopaschuk GD, Karwi QG, Tian R, Wende AR, Abel ED. Cardiac Energy Metabolism in Heart Failure. Circ Res. 2021 May 14;128(10):1487-1513.

[4] Ritchie RH, Abel ED. Basic Mechanisms of Diabetic Heart Disease. Circ Res. 2020 May 22;126(11):1501-1525

[5] Tong D, Schiattarella GG, Jiang N, Altamirano F, Szweda PA, Elnwasany A, Lee DI, Yoo H, Kass DA, Szweda LI, Lavandero S, Verdin E, Gillette TG, Hill JA. NAD+ Repletion Reverses Heart Failure With Preserved Ejection Fraction. Circ Res. 2021 May 28;128(11):1629-1641.

[6] Deng Y, Xie M, Li Q, Xu X, Ou W, Zhang Y, Xiao H, Yu H, Zheng Y, Liang Y, Jiang C, Chen G, Du D, Zheng W, Wang S, Gong M, Chen Y, Tian R, Li T. Targeting Mitochondria-Inflammation Circuit by β-Hydroxybutyrate Mitigates HFpEF. Circ Res. 2021 Jan 22;128(2):232-245.

[7] Tong M, Saito T, Zhai P, Oka SI, Mizushima W, Nakamura M, Ikeda S, Shirakabe A, Sadoshima J. Alternative Mitophagy Protects the Heart Against Obesity-Associated Cardiomyopathy. Circ Res. 2021 Dec 3;129(12):1105-1121.

[8] Thapa D, Manning JR, Stoner MW, Zhang M, Xie B, Scott I. Cardiomyocyte-specific deletion of GCN5L1 in mice restricts mitochondrial protein hyperacetylation in response to a high fat diet. Sci Rep. 2020 Jun 30;10(1):10665.

[9] Le Page LM, Rider OJ, Lewis AJ, Ball V, Clarke K, Johansson E, Carr CA, Heather LC, Tyler DJ. Increasing Pyruvate Dehydrogenase Flux as a Treatment for Diabetic Cardiomyopathy: A Combined 13C Hyperpolarized Magnetic Resonance and Echocardiography Study. Diabetes. 2015 Aug;64(8):2735-43.

[10] Gopal K, Al Batran R, Altamimi TR, Greenwell AA, Saed CT, Tabatabaei Dakhili SA, Dimaano MTE, Zhang Y, Eaton F, Sutendra G, Ussher JR. FoxO1 inhibition alleviates type 2 diabetes-related diastolic dysfunction by increasing myocardial pyruvate dehydrogenase activity. Cell Rep. 2021 Apr 6;35(1):108935.

[12] Zhang X, Ji R, Liao X, Castillero E, Kennel PJ, Brunjes DL, Franz M, Möbius-Winkler S, Drosatos K, George I, Chen EI, Colombo PC, Schulze PC. MicroRNA-195 Regulates Metabolism in Failing Myocardium Via Alterations in Sirtuin 3 Expression and Mitochondrial Protein Acetylation. Circulation. 2018 May 8;137(19):2052-2067.

[13] Davidson MT, Grimsrud PA, Lai L, Draper JA, Fisher-Wellman KH, Narowski TM, Abraham DM, Koves TR, Kelly DP, Muoio DM. Extreme Acetylation of the Cardiac Mitochondrial Proteome Does Not Promote Heart Failure. Circ Res. 2020 Sep 25;127(8):1094-1108.

[14] Scott I, Sack MN. Rethinking Protein Acetylation in Pressure Overload-Induced Heart Failure. Circ Res. 2020 Sep 25;127(8):1109-1111.

FIGURES

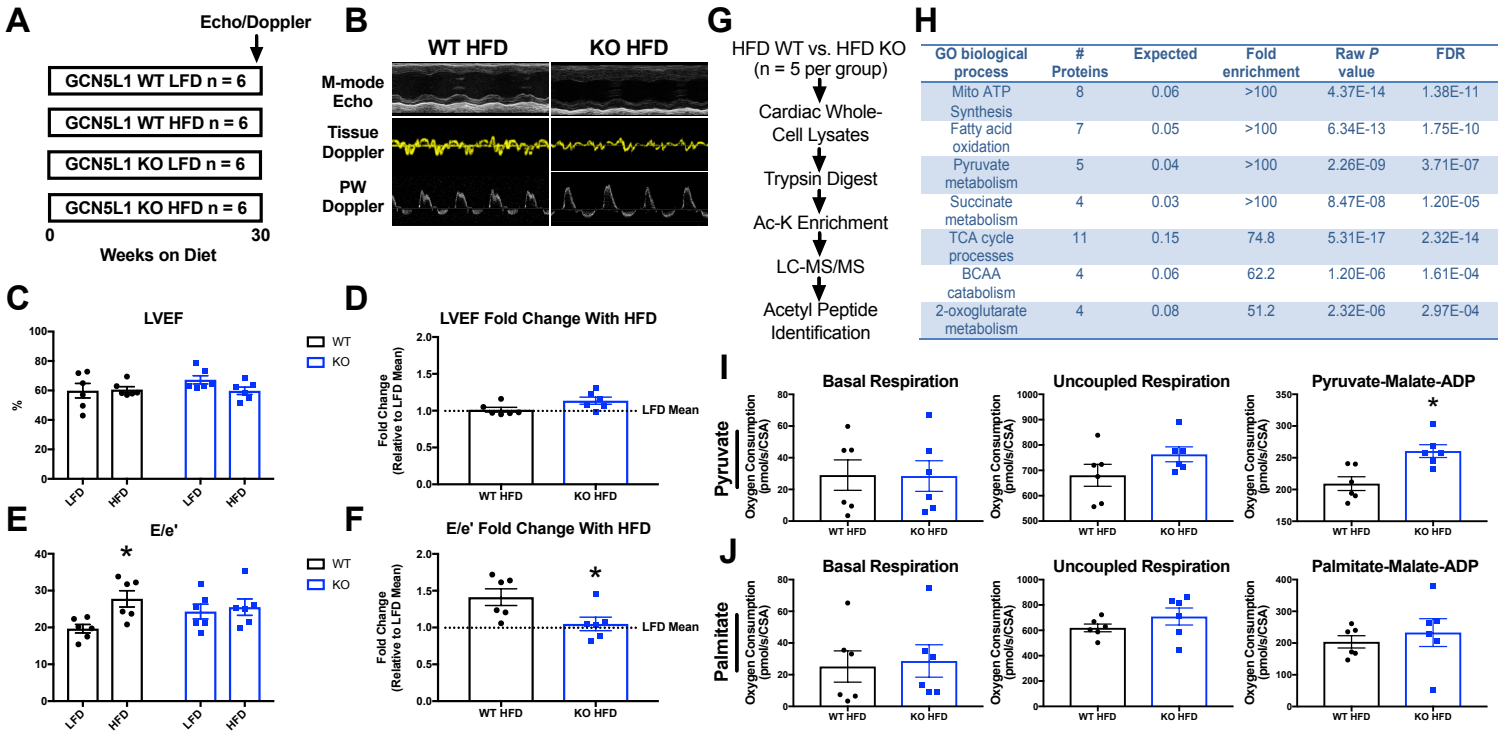

GO biological process	# Proteins	Expected	Fold enrichment	Raw *P* value	FDR
Mito ATP Synthesis	8	0.06	>100	4.37E-14	1.38E-11
Fatty acid oxidation	7	0.05	>100	6.34E-13	1.75E-10
Pyruvate metabolism	5	0.04	>100	2.26E-09	3.71E-07
Succinate metabolism	4	0.03	>100	8.47E-08	1.20E-05
TCA cycle processes	11	0.15	74.8	5.31E-17	2.32E-14
BCAA catabolism	4	0.06	62.2	1.20E-06	1.61E-04
2-oxoglutarate metabolism	4	0.08	51.2	2.32E-06	2.97E-04

Figure 1 – GCN5L1 promotes diastolic dysfunction and inhibits pyruvate oxidation in mice. A. Wildtype (WT) and cardiomyocyte-specific GCN5L1 knockout (KO) mice were placed on low fat (LFD), or high fat diets (HFD) for 30 weeks. **B-F.** Ultrasonography measurements of systolic (left ventricle ejection fraction; LVEF) and diastolic function (mitral valve E/e' wave ratio). N = 6; Two-way AVOVA (C & E) or T-test (D & F); * = $P < 0.05$. **G-H.** Quantitative acetylproteomics were used to identify biological pathways that were subject to GCN5L1-mediated lysine acetylation in HFD mouse hearts. GO enrichment analysis, *P* values, and False Discovery Rates (FDR) were calculated using PANTHER. **I-J.** Oxygen consumption in cardiac tissues from HFD-fed WT and KO mice was measured in response to either pyruvate-malate-ADP or palmitate-malate-ADP using Oroboros respirometry. N = 6; T-test; * = $P < 0.05$.

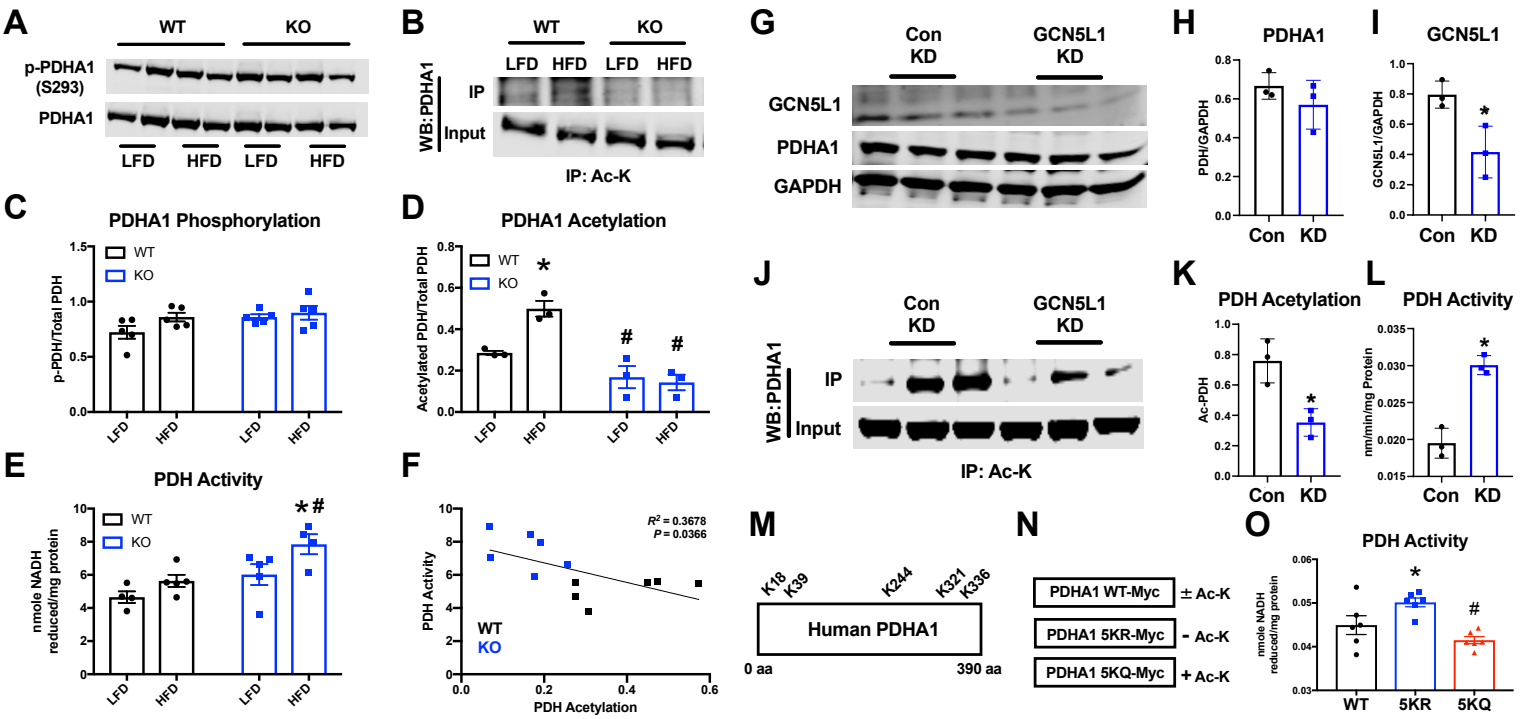

Figure 2 – GCN5L1 promotes PDHA1 acetylation and inhibits pyruvate dehydrogenase activity. **A-D.** PDHA1 phosphorylation (S293) and lysine acetylation in WT and KO mice following LFD or HFD. N = 3-5; Two-way ANOVA; * = $P < 0.05$ relative to WT LFD, # = $P < 0.05$ to WT HFD **E.** PDH activity in WT and KO mice following LFD or HFD. N = 3-5; Two-way ANOVA; * = $P < 0.05$ relative to WT LFD, # = $P < 0.05$ to WT HFD. **F.** Linear regression of PDH activity and acetylation levels in WT and KO mice following LFD or HFD. **G-L.** Total PDH acetylation and enzymatic activity was measured in stable Control shRNA or GCN5L1 shRNA knockdown (KD) human cardiac AC16 cells. N = 3; T-test; * = $P < 0.05$ relative to WT. **M.** Schematic of human PDHA1 showing published lysine acetylation sites. **N-O.** GCN5L1 KD AC16 cells were transfected with Myc-tagged wildtype PDHA1 (WT-Myc), a non-acetylated PDHA1 mimic in which lysines K18/K39/K244/K321/K336 were replaced with arginine (5KR-Myc), and an acetylated PDHA1 mimic where lysines K18/K39/K244/K321/K336 were replaced with glutamine (5KQ-Myc). N = 6; One-way ANOVA; * = $P < 0.05$ relative to WT, # = $P < 0.05$ to 5KR.

SOURCES OF FUNDING

This work was supported by: NIH/NHLBI K99/R00 (HL146905) to DT; NIGMS T32 (GM133332) to B.A.S.M; and NIH/NHLBI R01 (HL132917 & HL147861) research grants to IS. The University of Pittsburgh Center for Metabolism and Mitochondrial Medicine is supported by a Pittsburgh Foundation (MR2020 109502) grant to MJJ. The University of Pittsburgh Rodent Ultrasonography Core received support from the NIH/OD S10 Instrumentation Program (OD023684).

DISCLOSURES

None

AUTHOR CONTRIBUTIONS

Performed experiments: DT, PB, BASM, JRM, MWS, BM, XZ, PC, BX, LRE. **Designed experiments:** DT, PB, NY, MJJ, IS. **Analyzed data:** DT, PB, BM, XZ, PC, NY, BX, LRE, MJJ, IS. **Produced figures:** DT, PB, IS. **Wrote/edited manuscript:** DT, PB, NY, MJJ, IS.

SUPPLEMENTAL METHODS

Transgenic Mice

Cardiomyocyte-specific inducible GCN5L1 knockout (GCN5L1 KO) mice used in the studies were generated as previously reported [S1]. Cardiomyocyte-specific GCN5L1 deletion was induced via tamoxifen injection (single 40 mg/kg IP injection) as previously performed [S1].

Animal Care and Experimental Diets

Animals were housed in the University of Pittsburgh animal facility under standard conditions with *ad libitum* access to water and food, and maintained on a constant 12h light/12h dark cycle. Male WT and GCN5L1 KO animals aged 10 weeks were fed either a standard low fat diet (LFD; 70% carbohydrate, 20% protein, 10% fat; Research Diets D12450B), or a high fat diet (HFD; 20% carbohydrate, 20% protein, 60% fat; Research Diets D12492), for 30 weeks. At the end of 30 weeks, animals underwent ultrasonography, after which they were euthanized and heart tissues excised for analysis. Experiments were conducted in compliance with National Institutes of Health guidelines, and followed procedures approved by the University of Pittsburgh Institutional Animal Care and Use Committee.

Ultrasonography

65 Animals were anesthetized using isofluorane and monitored for cardiac functional parameters using a
66 VisualSonics Vevo 3100 in M-mode echocardiography, Tissue Doppler, and Pulsed-Wave Doppler
67 modes. Markers of systolic and diastolic function were calculated using standard echocardiography
68 equations.
69
70 **Quantitative Acetylproteomics**
71
72 Flash-frozen left ventricle tissues were homogenized in sodium deoxycholate (SDC) lysis buffer using
73 a bead mill (3 x 60 s at 6.5 s/m), and sonicated for 15 minutes in a water bath to shear DNA.
74 Extracted proteins (1.5 mg) were reduced (DTT) and alkylated (CAA), the SDC buffer removed by
75 acid precipitation, and desalted with Sep-Pek C18. After in-solution trypsin digest, 95% of the sample
76 was enriched using the acetyl PTMScan Kit (Cell Signaling). Peptides were eluted twice, and
77 desalted using PepClean C18 (Pierce). Peptides were subject to LC/MS/MS, and the data analyzed
78 using the MaxQuant software suite and Matlab-based script developed in-house. The ratio of acetyl-
79 peptide enrichment between WT HFD and KO HFD samples was determined for each detected
80 mitochondrial peptide, and all peptides where WT acetylation was greater than KO acetylation were
81 selected (Table S1). Identified genes corresponding to these peptides were entered into the
82 PANTHER gene ontology search engine (www.geneontology.org), and grouped according to
83 functional class. Functional classes containing ≥ 4 independent genes were selected for analysis. *P*
84 values, fold enrichment, and false discovery rates were determined by PANTHER.
85
86 **Respirometry**
87

Citrate synthase activity was determined by preparing a mitochondrially-enriched supernatant by homogenizing a 50 mg piece of left ventricle in 1 ml of STE buffer (250 mM sucrose, 10 mM Tris-HCl, 1 mM EDTA) with a glass vessel and Teflon pestle, followed by centrifugation at 800 *g* for 10 min at 4 °C. Citrate synthase activity was then measured by mixing the mitochondrially-enriched fraction with citrate synthase activity buffer (0.25% Triton X-100, 0.31 mM acetyl-CoA, 0.1 mM 5,5'-dithiobis(2-nitrobenzoic acid), 0.1 M triethanolamine, 1 mM EDTA, and 1 M Tris-HCl), followed by addition of 5 mM oxaloacetate to initiate the reaction. The change in absorbance at 412 nm was recorded every 10 seconds over a two-min period using a spectrophotometer set to 37 ^{o}C, and activity was calculated as the slope from the linear portion of the curve and normalized to the protein concentration determined by BCA protein assay. Citrate synthase activity was used to normalize respirometry measurements. Respirometry was performed using an Oroboros O2K High-Resolution Respirometer using mitochondrially-enriched cardiac samples prepared as described above. Respiration was measured in MiR05 buffer at 37 ^{o}C under constant mixing in a sealed, 2 ml chamber. The respirometry protocol consisted of sequential additions of substrates and inhibitors as follows: pyruvate (5 mM) or BSA-conjugated palmitate (0.25 mM), malate (2 mM), ADP (2 mM); oligomycin (2.5 μM); carbonyl cyanide 4-(trifluoromethoxy)phenylhydrazone (FCCP; titrations of 0.5 μM until maximal respiration reached); antimycin A (2.5 μM). Protein concentration of the mitochondrially-enriched fraction was determined by BCA protein assay, and oxygen consumption or flux expressed per mg protein normalized to citrate synthase activity.

Cell Culture and Transfection

Stable control shRNA and GCN5L1 shRNA AC16 cells were described previously [S3]. WT PDHA1-Myc, 5KR PDHA1-Myc, and 5KQ PDHA1-Myc were produced using custom gene synthesis by Genscript, and cloned into the pCMV-3Tag-4a plasmid vector. Cells were transfected for 24 h using X-tremeGENE reagent.

Protein Isolation, Western Blotting, and Immunoprecipitation

For western blotting, tissues were minced and lysed in CHAPS buffer (1% CHAPS, 150 mM NaCl, 10 mM HEPES, pH 7.4) on ice for ~2 hours. Homogenates were spun at 10,000 *g*, and supernatants were collected. Protein lysates were prepared in LDS sample buffer, separated using Bolt SDS/PAGE 4-12% or 12% Bis-Tris gels, and transferred to nitrocellulose membranes (all Life Technologies). Protein expression was analyzed using the following primary antibodies; rabbit PDHA1 Ser-293 antibody (Cell Signaling; #31866), rabbit PDHA1 (Cell Signaling; #3205), and rabbit GAPDH (Cell Signaling; #2118). GCN5L1 antibody was made by Covance and previously validated [S2]. Fluorescent anti-mouse or anti-rabbit secondary antibodies (red, 700 nm; green, 800 nm) from Li-Cor were used to detect expression levels. Protein densitometry was measured using Image J software (National Institutes of Health, Bethesda, MD).

For immunoprecipitation experiments, tissues were minced and lysed in CHAPS buffer (1% CHAPS, 150 mM NaCl, 10 mM HEPES, pH 7.4) on ice for ~2 hours. Homogenates were spun at 10,000 *g*, and supernatants were collected. Protein lysates were incubated overnight at 4 ºC with rabbit acetyl-lysine (Ac-K, #9441) from Cell Signaling Technology. Immunocaptured proteins were isolated using Protein-G agarose beads (Cell Signaling Technology, #9007), washed multiple times with CHAPS buffer, and

then eluted in LDS sample buffer (Life Technologies) at 95 ºC. Samples were separated on 12% Bis-Tris Bolt gels and probed with appropriate antibodies. Protein densitometry was measured using Image J software (National Institutes of Health, Bethesda, MD).

Biochemical Assays

PDH activity was assessed using a commercial kit (MAK-183; Sigma-Aldrich) according to the manufacturer's instructions.

Statistics

Graphpad Prism software was used to perform statistical analyses. Means ± SEM were calculated for all data sets. Data were analyzed using two-way ANOVA with Tukey's post-hoc multiple comparison testing to determine differences between genotypes and feeding groups. Data were analyzed with two-tailed Student's T-tests to determine differences between single variable groups. $P < 0.05$ was considered statistically significant.

Supplemental References

[S1] Thapa D, Manning JR, Stoner MW, Zhang M, Xie B, Scott I. Cardiomyocyte-specific deletion of GCN5L1 in mice restricts mitochondrial protein hyperacetylation in response to a high fat diet. Sci Rep. 2020 Jun 30;10(1):10665.

[S2] Scott I, Webster BR, Li JH, Sack MN. Identification of a molecular component of the mitochondrial acetyltransferase programme: a novel role for GCN5L1. Biochem J. 2012 May 1;443(3):655-61.

[S3] Manning JR, Thapa D, Zhang M, Stoner MW, Traba J, Corey C, Shiva S, Sack MN, Scott I. Loss of GCN5L1 in cardiac cells disrupts glucose metabolism and promotes cell death via reduced Akt/mTORC2 signaling. Biochem J. 2019 Jun 19;476(12):1713-1724.